Ultralow-Temperature Sintering of CP-Titanium by Spark Plasma Sintering under Cyclic Pressure

Nao Manabe [a], Ayako S. Suzuki [b], Mei Ninagawa [a], Hideki Wakabayashi [c], Naomi Hirayama [c], Kouichi Niinobe [d], Yuanbo T. Tang [e,f], Satoshi Utada [e,g], D. Graham McCartney [c,e], Roger C. Reed [c,e,h], Hiroyuki Kitagawa [a,c,*]

[a] Department of Physics and Materials Science, Shimane University, Matsue 690-8504, Japan

[b] S. S. Alloy Co., Ltd., 3-13-26 Kagamiyama, Higashi-Hiroshima 739-0046, Japan

[c] Next Generation Tatara Co-Creation Centre (NEXTA), Shimane University, Matsue 690-8504, Japan

[d] Department of Mechanical Engineering, National Institute of Technology, Matsue College, Matsue 690-8518, Japan

[e] Department of Materials, University of Oxford, Parks Road, Oxford OX1 3PH, United Kingdom

[f] School of Metallurgy and Materials, University of Birmingham, Elms Road, Birmingham B15 2SE, United Kingdom

[g] National Institute for Materials Science, 1-2-1 Sengen, Tsukuba 305-0047, Japan

[h] Department of Engineering Science, University of Oxford, Parks Road, Oxford, OX1 3PJ, United Kingdom

***Corresponding Author.**

E-mail address: kitagawa@riko.shimane-u.ac.jp (H. Kitagawa)

Abstract

Spark plasma sintering (SPS) is a promising method for producing titanium components from powder but a limitation is that high sintering temperatures (> 900 °C) are normally required to eliminate porosity. Here we report the SPS of titanium powder using both cyclic and constant uniaxial pressure and compare densification, microstructure and mechanical behavior. The following parameters were varied: sintering temperature, T_S, 400 to 900 °C; cyclic and constant pressures, 100 to 500 MPa; with and without an isothermal dwell of 60 minutes at T_S. The mechanical behavior was determined by bend and tensile testing. We demonstrate that the application of cyclic pressure (cyclic-SPS) gives superior densification of CP-titanium powder over the range of parameters investigated compared with a constant pressure. Bend testing reveals improved ductility after cyclic-SPS compared with a constant pressure. The dwell at T_S further improves mechanical properties, giving excellent tensile ductility and strength. Consequently, at the ultralow temperature of 500 °C, nearly fully dense, ductile, titanium is achieved. We show that cyclic pressure enhances the degree of powder compaction at room temperature, and we propose mechanisms to rationalize the effect of cyclic-SPS on enhancing the rates of densification and sintering as the temperature increases during processing.

Keywords: spark plasma sintering, titanium, densification, mechanical properties

1. Introduction

Spark plasma sintering (SPS), which is also called pulsed electric current Sintering (PECS) or field assisted sintering technique (FAST), is well known as a pressure sintering method that allows rapid sintering at low temperatures because of direct heating of the raw powder and the die by applying a pulsed electric current [1-4]. In recent years, the advantages of SPS have been reviewed by several authors [5-9]. According to these reviews, SPS allows materials to be sintered at lower-temperatures and shorter-times compared with conventional sintering methods (for example pressure-less sintering, hot pressing (HP) and hot isostatic pressing (HIP)) and to obtain dense (i.e. low porosity) sintered materials whilst controlling grain growth and chemical reaction. Due to these features, SPS has been applied to a wide variety of materials, including metals, intermetallics, ceramics, carbon materials, functionally graded materials and so on.

Titanium (Ti) and related alloys are important as engineering materials for many applications due to their low density, high tensile strength, and good corrosion resistance. Therefore, several studies have focused on the SPS of Ti and related alloys [10-22]. It is well known that Ti has a hexagonal to cubic (α to β) phase transformation at approximately 880 – 890 °C [10, 23-24]. In many cases, regardless of the powder particle size or grade of Ti, the sintering temperature of Ti by conventional SPS is over 800 °C, which is close to or even above this transformation temperature. Some researchers have noted that this phase transformation affects the densification behavior of Ti [10-12] and increases the final grain size of the product. Zadra *et al*. studied the SPS of both gas atomized powder (<45 μm) and

hydrogenated dehydrogenated powder (<45 μm) of Ti [10]. According to their study, Ti powder was densified to 99 % theoretical density (TD) at 800 °C and was fully densified at a sintering temperature of 950 °C for 5 min under 60 MPa of static pressure. They also reported that a sintering temperature of 900 °C is the best condition to obtain excellent mechanical properties and microstructure. Eriksson *et al*. performed a systematic investigation of the sintering behavior of Ti powder (< 44 μm) by SPS at various sintering temperatures (from room temperature to 950 °C without a dwell time) under various pressures (10~100 MPa) [11]. Their experimental results clearly show that a sintering temperature of 750 °C or higher is required to obtain a nearly fully dense material (99.0 % TD) even though the pressure was increased up to 100 MPa, which is a relatively high pressure as the conventional SPS process typically uses a graphite die. Bustillos *et al*. recently investigated the SPS of the Ti-6Al-4V alloy [25]. Powder was sintered at 600~650 °C for 10 min and with a high pressure of 300~555 MPa. According to their results, the relative density of sintered materials reached 99 %TD at 650 °C and 555 MPa. This sintering temperature appears to be, at present, the lowest reported in the literature to obtain the full densification of Ti and related alloys.

We have recently developed the technique of spark plasma sintering under a uniaxial cyclic pressure and experiments on bismuth telluride, a thermoelectric material, are described in reference [26]. In this new densification/sintering method, the powder is sintered by applying a cyclic pressure produced by moving the punch up and down during pulsed current heating. In addition to the advantages of conventional SPS, this cyclic pressure method allows us to have other advantages that could not be

achieved by conventional SPS. For example, it has been shown to be effective in controlling the texture of Bi_2Te_3-related thermoelectric materials [27] and it has also been used to produce a range of controlled microstructures by optimized selection of the process parameters (e.g. sintering temperature and dwell time) [28]. In addition, some researchers have reported that an oscillating pressure application during a hot press sintering enhances the densification and sintering of the metals [29-30] and ceramics powders [31]. Therefore, our modified SPS method, involving cyclic pressure application, appears to be promising for the synthesis and improved low temperature densification of various materials, including ceramics, composites, and metals such as Ti.

To date, neither CP-Ti nor Ti-6Al-4V powders have been fully densified below 600 °C. If the densification of Ti could be attained at low temperatures (<600 °C) by cyclic pressure application, there is the potential to achieve grain refinement and minimize chemical reaction since the α-β phase transformation of Ti will not occur during processing. In a recent paper [32], we reported the enhancement of the densification of CP-Ti (over 95%TD at 500 °C) by applying a uniaxial cyclic pressure during SPS. In the light of this initial study, the main aim of the present work reported was to conduct a more comprehensive investigation into how the application of cyclic pressure during SPS influences (i) the densification and sintering behaviors of CP-Ti, and (ii) the resultant mechanical properties of the sintered compact.

Here we provide new results on the application of cyclic uniaxial pressures from 100-500 MPa in the temperature range 400 to 900 °C as well as the effect of a dwell time as part of the sintering cycle.

Following the sintering experiments, density measurements and microstructural characterization were undertaken and the mechanical properties were determined; qualitatively by simple bend tests, and quantitatively using a miniaturized tensile test. The factors contributing to the densification of CP-Ti during SPS with a cyclic pressure, and the effect of process parameters on the tensile behavior are discussed.

2. Experimental Methodology

2.1 Materials and spark plasma sintering (SPS) processing

The powder used in the present study was a gas-atomized near-spherical powder of CP-Ti (TILOP-45; OSAKA Titanium Technologies Co. Ltd) with the following nominal composition: 0.121 wt% O, 0.027 wt.% Fe, 0.003 wt% N, 0.004 wt% H and 0.002 wt% C, this chemical composition is within a range of grade 1. The approximate α and β transus temperature for grade 1 CP-Ti is 890 °C [10]. The powder had a nominal particle size below 45 μm with a median of 22.5 μm.

Spark plasma sintering (SPS) experiments were performed in a PLASMAN CSP-III-1012DP apparatus (S.S. Alloy Co. Ltd., Higashi-Hiroshima, Japan) at temperatures ranging from 400 to 900 °C under constant and cyclic uniaxial sintering pressures of 100, 300 and 500 MPa with a chamber pressure of <10 Pa. Either a continuous cyclic uniaxial pressure (0 to a maximum pressure of 100, 300 or 500 MPa) or a constant pressure of 100, 300, 500 MPa was applied during the sintering.

Due to the high temperatures and pressures involved, die and punches were made from a WC-FeAl cemented carbide (as opposed to the normal graphite) because of its high temperature mechanical strength and electrical resistance for pulsed current heating.

In the constant pressure experiments, the powder was loaded into the die, the desired sintering pressure was applied before heating was begun and held until the end of the temperature cycle. For the cyclic pressure experiments, the pressure was applied and then removed by raising the punch by approximately 3 mm at a frequency of approximately 0.25 Hz throughout the temperature cycle, Fig. 1 (a) and (b). Samples were produced as either 10 mm diameter x 3 mm discs (for monitoring the densification process) or 10 mm diameter x 13 mm cylinders (for the manufacture of tensile test pieces).

In both processes, a K-type thermocouple was inserted into a hole on WC-FeAl die wall to monitor the temperature during SPS processing and the sintering temperatures given in the present paper refer to those measured by the thermocouple.

The aim of the present work was to investigate the influence of the following variables namely: sintering temperature, cyclic/constant pressure, and dwell time at the sintering temperature. The temperature programs for the SPS experiments are shown in Fig. 1(c). The heating rate was approximately 50 $Kmin^{-1}$ to a temperature 20 K lower than the target sintering temperature and after that 10 $Kmin^{-1}$ to avoid overshooting. The samples were either heated to the desired temperature (between 400 – 900 °C) and immediately cooled naturally or held for a dwell time of 60 min at the target sintering temperature followed by natural cooling to room temperature. The sintering

experiments without a dwell time were undertaken using the combination of experimental parameters shown in Table 1. The higher-pressure sintering experiments had to be limited to lower temperature ranges due to the safe design limitations of the die material. To investigate the effect of a dwell time at the sintering temperature the combination of process parameters employed is listed in Table 2.

The density of the sintered samples was determined by the Archimedes method for samples with a relative density of 90%TD or more and by the measurement of sample dimensions for those with a relative density less than 90%TD. In the Archimedes method, the samples were soaked in water prior to measurement to eliminate any air bubbles present. To measure sample dimensions, samples were

Table 1 Combination of process parameters used in the SPS experiments with no dwell time at the sintering temperature.

Temperature / °C	Pressure / MPa					
	100		300		500	
	constant	cyclic	constant	cyclic	constant	cyclic
900	○					
700	○	○				
600	○	○	○	○		
500	○	○	○	○		
400	○	○	○	○	○	○

Table 2 Combination of process parameters used in the SPS experiments with a 60 min dwell at the sintering temperature.

Temperature / °C	Pressure / MPa					
	100		300		500	
	constant	cyclic	constant	cyclic	constant	cyclic
700	○	○				
600	○	○				
500	○	○	○	○		
400					○	○

lightly polished to remove burrs, and then diameter and thickness were measured by a micrometer.

The relative density was computed from the known density of CP Ti which is taken as 4506 kg/m^3 and is reported in the paper as a percentage of theoretical density (TD).

2.2 Materials characterization

Cross-sections of sintered samples were prepared by cutting with a diamond slitting wheel from the sample discs. The cross-section was then hot mounted, sequentially ground using a resin bonded diamond grinding disc and then polished to a 9 μm diamond surface finish. Final polishing was undertaken using 0.25 μm colloidal silica suspension. The microstructure was observed by polarized light mode of optical microscopy. The grain size of samples was measured on cross-sections using the line intercept method with an average of 15 measurements on each sample. For investigation by electron backscatter diffraction (EBSD), the polished samples were chemically etched in Kroll's reagent (1 ml HF, 4 ml HNO_3, 50 ml H_2O). The measurements were performed with a JIB-4700F field emission SEM (JEOL) equipped with a Symmetry S2 EBSD detector and AZTEC data acquisition and analysis software (Oxford Instruments Nanoanalysis) with an accelerating voltage of 15 kV and beam current of 5 nA. The observed area was approximately 400 x 300 μm with a step size of 1 μm.

Microhardness values were measured with an HMV-G-FA-D (Shimadzu) microhardness instrument with a diamond Vickers indenter using a 5 N (0.5 kgf) load and a dwell time of 15 s for each indentation. The values reported are the mean of ten indentations on each sample.

To obtain more information about the mechanical behavior and sintered microstructure, samples of dimensions approximately 1 x 3 x 10 mm were cut from sintered discs and were deformed by bending.

The fracture surfaces of samples that failed after bending were examined in a TM4000 Plus (Hitachi High-Technologies) SEM operating at 15 kV in the secondary electron mode. Representative samples from the bending experiments, one which showed ductile behavior and deformed without failing and another which showed brittle behavior and fractured without significant plastic deformation are shown in Fig. 2.

2.3 Tensile testing of SPS samples

Based on the initial observations on microstructure, porosity, and bending experiments, the room temperature tensile behavior of samples from selected SPS processing conditions was determined. Tensile testing was performed using an Instron Electro-Thermal Mechanical Testing (ETMT) system, equipped with a 5 kN load cell capable of testing samples of small size. Specimens were first electro discharge machined from the sintered cylinders of dimensions 10 mm diameter x 13 mm into a dog bone shape test piece with a total length of 13 mm and a gauge cross-sectional area of ~ 2 × 0.5 × 5 mm. Recast layers induced by such machining were subsequently removed using abrasive media, finishing with 4000-grit paper. Dimensions were then measured using a micrometer with a precision of 1 μm. The specimen was mounted between two grips. The strain measurement was conducted using a non-contacting digital image correlation video extensometer, where a speckle pattern is applied to the surface of the specimen with white and then black paint for video extensometer tracking purposes. The video data were recorded at 10 Hz and analyzed using the Imetrum Video Gauge software. Tensile

loading was carried out at a strain rate of $\sim 10^{-3}$ s^{-1} until failure. Two samples were tested for each of the SPS processing conditions investigated.

3. Results

3.1 Densification measurements

Figure 3 shows the dependence of the relative density of CP-Ti on the sintering temperature under various constant/cyclic pressure cycles without an isothermal dwell time. Fig. 3(a) displays the entire measured range and Fig. 3(b) an enlarged view of the higher density region of the plot. As shown in Fig. 3(a), regardless of the magnitude of the applied pressure, the relative density of the Ti was enhanced at lower temperatures by applying a cyclic pressure instead of a constant pressure. Moreover, Fig. 3(b) clearly reveals that the density of Ti reached 99.5 %TD at low temperatures (below 700 °C) by applying a cyclic pressure of 100, 300 or 500 MPa; 99.5%TD is conventionally considered full densification. Notably, full densification was achieved at a temperature of only 300 °C by applying a cyclic pressure of 500 MPa.

3.2 Microstructure and microhardness investigations

Figure 4 (a) shows optical micrographs of powder that was sintered by SPS at temperatures from 400 to 900 °C under various constant and cyclic pressures. A pressure of 100 MPa was applied for sintering temperatures above 600 °C, 300 MPa for a temperature of 500 °C and 500 MPa for 400 °C; the dwell time was set to be either 0 or 60 min. For samples sintered without a dwell time, the grain

size is not significantly affected by the loading condition except at 700 °C. However, when held for 60 min the grain size is noticeably coarser when cyclic pressure is applied at 600 and 700 °C. In addition, pores in the sintered material, that are typically observed at the positions indicated by arrows, tended to decrease in number when using cyclic pressure compared with constant pressure, Fig.4 (b). This is consistent with the relative density improvement (Fig.3 (b)).

Figure 5 shows a plot of the grain size measurements determined by the line intercept method at sintering temperatures of 400 - 900 °C with constant and cyclic pressures. The data for samples without an isothermal dwell time, and sintered below 700 °C, show a grain size of around 10 μm regardless of the pressure cycle. However, it is notable that in the constant pressure sample sintered at 900 °C (i.e. above the α/β transus temperature) the grain size was larger ~ 40 μm. The data for a 60 min dwell show that the grain size is only slightly increased with application of a constant pressure up to 700 °C. In contrast, with a cyclic pressure, the grain size increased significantly for 600 and 700 °C sintering temperatures but remained around 10 μm for lower temperatures.

Figure 6 shows the relationship between Vickers microhardness $H_{V0.5}$ and relative density for samples processed under different conditions and reveals that the microhardness increases with relative density, i.e. as the porosity of the sample decreases, and is almost independent of the grain size within the observed range. The $H_{V0.5}$ value of sintered samples having density > 99% was approximately 150 $H_{V0.5}$, which is a typical value of sintered grade 1 CP-Ti [10].

3.3 Mechanical behavior under bending and tensile testing

In Figure 7, results are shown that reveal the effect on the microstructure and the mechanical behavior of applying a cyclic versus a constant pressure (100 MPa) at three different sintering temperatures without a dwell time. Fig. 7(a) shows the fracture surfaces following bending of samples sintered at 500, 600 and 700 °C with constant and cyclic pressures of 100 MPa. Ductile fracture surfaces, with clearly evident dimpled fracture features, were obtained at 700 °C regardless of the pressure conditions. At 500 °C, brittle fracture occurred and there is little evidence for interparticle bonding on the fracture surface of either cyclic or constant pressure samples. However, when sintered at 600 °C, a ductile fracture was promoted by applying a cyclic pressure. The fracture surface in the sample processed with a cyclic pressure shows clear evidence for interparticle bonding although it does not have classical ductile dimples.

To understand the deformation behavior better, tensile tests were performed on the samples sintered at 700 °C and 600 °C. The engineering stress – strain plots are shown in Fig. 7 (b). The sample sintered at 700 °C under cyclic conditions had the highest ultimate tensile strength (UTS) and elongation to failure. The tensile testing results correlate well with the fracture surface features as all three plots show a significant degree of plasticity after the onset of necking at the UTS. The 600 °C sample sintered with a cyclic pressure exhibits the lowest elongation to failure and post-UTS ductility, in line with the fracture surface of the bend test sample that revealed less ability to develop localized dimples.

Fig. 8 (a) shows the fracture surfaces of samples sintered at 500 and 600 °C under 100 and 300 MPa cyclic and constant pressures without a dwell time. At 300 MPa, ductile fracture surfaces, with clearly

defined dimpled features, are found after sintering at 600 °C but not at 500 °C. At 500 °C, there is a flattening of the interparticle contacts, which is more evident in the sample processed under cyclic conditions, but evidence for interparticle bonding is limited.

At 100 MPa and 600 °C, there is a notable effect of the application of cyclic pressure compared to a constant pressure. Only the sample processed with cyclic pressure had a ductile fracture at 600 °C in the bend test. The fracture surface of this sample exhibits features of ductile tearing, but not well formed ductile dimples, suggesting that extensive interparticle bonding had not been achieved. However, at 100 MPa and 500 °C, the near-spherical morphology of the original powder particles is still evident with only slight evidence of particle flattening at points of contact irrespective of the pressure conditions. In Fig. 8 (b) the tensile test plots for samples with a cyclic pressure applied show good correlation with the corresponding bend test fracture surface features. The higher UTS and greater elongation to failure of the 300 MPa/600 °C sample compared to the 100 MPa/600 °C sample are consistent with the more well-developed ductile dimple features of the fracture surface of the former.

In Fig. 9 the effects of dwell time, sintering temperature and cyclic sintering pressure on the mechanical behavior are revealed through the fracture surface features of bend test samples and tensile stress – strain plots. Fig. 9 (a) shows that SPS at 600 °C/100 MPa and 700 °C/100 MPa with a dwell time leads to fracture surfaces that display a greater degree of ductile-dimple character than without a dwell. This presumably indicates enhanced interparticle bonding when a dwell time is used. However,

with SPS at 500 °C/100 MPa only when a dwell time was used does the fracture surface of the sample exhibit some evidence of ductile tearing features; nevertheless this processing condition was sufficient to allow plastic bending. When the pressure was increased to 300 MPa at 500 °C the fracture surface of the sample with a dwell time shows a significant transition to a ductile-dimple character. However, without a dwell, the fracture surface appeared brittle in character with minimal evidence for interparticle bonding. In the case of SPS at 400 °C/500 MPa, although the samples were found to be nearly fully dense (with 99.5%TD, Fig.3), the fracture surface had a brittle appearance (no ductile dimples or ductile tearing), and even after a 60 min dwell particle bonding was apparently insufficient to give ductility. Finally, the differences in fracture surface appearance following bending correlate well with the representative tensile test plots shown in Figs. 9 (b) and (c). The improved tensile behavior (greater UTS and tensile ductility) of the 600 °C/100 MPa sample following a dwell time is clearly evident in Fig. 9(b). In Fig. 9(c), the 500 °C/300 MPa and 600 °C/100 MPa SPS samples, both with a dwell time, show almost identical tensile behavior. Whilst the plot obtained from the 700 °C/100 MPa sample shows the highest UTS, it has a somewhat unexpectedly reduced elongation to failure. The fracture surface of the 700 °C/100 MPa sample in Fig. 9(a) shows a larger grain size (also clear in the cross-sectional microstructure, Fig. 4) and this might play a role in the reduced ductility seen in the tensile test. The mechanical property measurements from the tensile tests undertaken in this study are summarized listed in Table 3. For comparison, mechanical property data obtained from CP-Ti

powder processed by conventional SPS and the value for sintered grade-1 CP-Ti read from Zadra's report [10] is also listed.

Table 3 Young's modulus (YM), 0.2% proof strength (0.2% PS), ultimate tensile strength (UTS) and elongation to failure (El) for CP-Ti prepared under various SPS conditions.

Sintering conditions				YM / GPa	0.2% PS / MPa	UTS / MPa	El / %
Temperature / °C	Pressure / MPa	Time / min	Cyclic / Constant				
700	100	0	Cyclic	110	371	469	37
600	100	0	Cyclic	96	332	422	25
600	300	0	Cyclic	102	344	439	41
700	100	60	Cyclic	109	385	472	32
600	100	60	Cyclic	100	367	460	38
500	300	60	Cyclic	111	347	458	40
900	100	0	Constant	99	320	436	35
700	100	0	Constant	99	346	434	29
900	60	5	Constant [10]	-	343	445	39

4. Discussion

This study demonstrates that the application of a cyclic pressure (cyclic SPS) gives superior densification of CP-Ti over the entire range of process parameters investigated compared with a constant pressure. Bend testing of samples reveals improved ductility after cyclic SPS compared with equivalent constant pressure processing. A dwell time of 60 min during cyclic SPS is sufficient to further improve mechanical properties giving excellent tensile ductility and strength at 500 °C/300 MPa with an elongation to failure of 40 %, yield strength of 347 MPa and tensile strength of 458 MPa.

In the following sections, densification and sintering of Ti will be considered and reasons for the effectiveness of cyclic pressure application during SPS will be proposed. In addition, the evolution of the microstructure and the resultant mechanical properties will be rationalized and compared with previous work on the SPS of Ti.

4.1 Review of densification and sintering phenomena in SPS of Ti – the four stages

In the SPS of metal powders the densification and sintering that occur as the temperature is increased can generally be considered in terms of the following four stages: (i) rearrangement of the powder particles, (ii) localized plastic deformation of the powder at points of contact, (iii) bulk deformation of the compact and finally (iv) sintering by mass transport phenomena as the diffusion rate increases at higher temperatures [33-34]. Fig. 10 shows this sequence schematically.

In the processing of Ti by SPS, particle and bulk deformation are believed to be responsible for significant initial densification as the yield strength of CP-Ti decreases substantially with increasing temperature e.g. from 170 MPa at room temperature to 110 MPa at 200 °C and 76 MPa at 400 °C [35].

The sintering densification of Ti involves several interacting events as described by German [36]. First, local surface temperature must be above 700 °C to begin to remove surface oxide, then surface diffusion initiates the formation of interparticle bonds and grain boundary diffusion continues this process at the newly formed interparticle boundaries. As the relative density increases, bulk diffusion begins to become more important.

In processing by SPS, the phenomena induced by pulsed current heating are not well understood [37-40]. Nevertheless, a higher temperature which is localized at powder particle points of contact is thought to occur [7, 9, 41-43]. This will probably lead to more effective removal of oxide from the Ti metal surface and consequently enhance the interdiffusion between particles, the formation of a sintering neck, followed by growth of the neck and diffusion driven densification. Since the grain boundary and surface diffusion coefficients are much larger than the bulk self-diffusion coefficient in α-Ti [36], they could potentially be sufficiently large to permit densification at a lower temperature than in conventional furnace sintering. Alongside diffusion data, it is also necessary to consider microstructural features of the compact such as number of points of contact between the powder particles and the contact area between them. An increase in the number and size of the points of contact by deformation during SPS will be expected to enhance the densification rate through sintering. Also to be considered is the presence of lattice defects such as dislocations and low angle grain boundaries within the powder particles. These lattice defects could well induce more rapid diffusion that expected from bulk diffusion data [18, 44-45].

We will now consider how cyclic pressure could have affected the densification and sintering mechanisms proposed in the literature, and summarized above, for conventional SPS.

4.2 Effect of cyclic pressure application on densification and sintering phenomena in the four stages

First, it is necessary to consider how applying a cyclic pressure might affect the powder rearrangement and low temperature plastic deformation contributions (stages i and ii of densification). We conducted an additional experiment with a room temperature compression test to better understand this rearrangement as briefly set out in the Appendix A. Figure 11 shows the dependence of the relative density of the Ti compacts at room temperature on the number of applied pressure cycles for different pressures. The relative density of the compacts increased with increasing the number of pressure cycles at all levels of applied pressure. It is notable that the relative density of the compacts effectively reaches a plateau value after 10 or more cycles.

The cold compaction data from these experiments were analyzed with the well-known Cooper-Eaton approach [46] as set out in the Appendix B. Figure 12 shows an example of the compaction analysis, based on the Cooper-Eaton equation for an increasing pressure with a single cycle. The experimental values are well fitted based on the Cooper-Eaton equation and the compaction behavior can be interpreted in terms of two contributions [47-48]. The curve rapidly increasing at low pressure is due to the rearrangement of powder and the curve gradually increasing at higher pressure is attributed to plastic deformation. Figure 13 (a) shows the compaction curves for Ti powder for different numbers of pressure cycles and Table 4 lists the fitting parameters of A_1, A_2, B_1 and B_2.

Here, B_1 (the starting pressure for rearrangement) was set to be 1 for $N \geq 3$ because fitting was enabled for any value of $B_1 \leq 1$, indicating that rearrangement was rapidly completed by the repetitive

pressure application. For all curves, $A_1 + A_2$ is close to 1, confirming that powder compaction was dominated by the two processes of rearrangement and plastic deformation.

Table 4 Fitted parameters A_1, A_2, B_1, B_2 in the Cooper-Eaton equation, classified by N, the number of applied pressure cycles.

N	A_1	A_2	A_1+A_2	B_1 (MPa)	B_2 (MPa)
1	0.345	0.637	0.982	4.894	225
3	0.284	0.665	0.949	1	113
10	0.276	0.725	1.001	1	105
100	0.279	0.697	0.976	1	83
1000	0.28	0.703	0.983	1	81

It should be noted that A_2 (the fractional contribution from plastic flow) was increased and B_2 (the onset pressure for deformation) was decreased with an increasing number of repetitive pressure cycles. This strongly suggests that powder compaction through plastic deformation is enhanced by the cyclic pressure, even when the number of pressure cycles is as low as 3. Figure 13 (b) shows SEM images of the cold compressed powder at the four points I, II, III, IV on the curves in Fig. 13 (a) (shown by the arrows). In the case of one pressure cycle at 100 MPa, the plastic deformation of the powder particles has not evidently occurred, and spherical particles similar to the starting powder are seen. Even with a pressure up to 300 MPa, a significant change in particle morphology was not observed although the fractional volume compaction was increased (Fig. 13 (b) I and II). On the other hand, enhancement of plastic deformation was observed after both 100 cycles at 300 MPa and more noticeably after 1000 cycles at 500 MPa (Fig. 13 (b) III and IV).

These cold compaction experiments demonstrate the mechanisms of enhanced densification that are expected to occur in stages 1 and 2 (up to a temperature of around 300 °C) of densification in an SPS experiment when using a cyclic pressure. There were ~ 120 pressure cycles in these SPS stages and so an increased powder packing density, with an increase in the number of points of contact, is expected compared with a constant pressure. As the temperature increases further, the points of contact can deform plastically, increasing both the area per contact and total contact area compared with constant pressure. In the third stage of densification, above ~ 300 °C, bulk deformation of the compact will increasingly contribute to densification due to the decreasing yield strength of the Ti with increasing temperature (76 MPa at 400 °C [35]). In this bulk deformation stage, the role of cyclic pressure application is less clear. However, it is possible to suggest that dislocation structures during cyclic loading differ from those generated by constant loading and that dislocation density could be expected to increase with the number of plastic stress cycles [49]. Such an effect could increase the density of lattice defects within the powder particles and hence accelerate diffusion across particle boundaries.

Overall, an increase in the number and size of the points of contact and the increased presence of lattice defects at these contact points (introduced in stages 1 to 3 by cyclic pressure) could also accelerate stage (iv) of densification at temperatures from 500 °C upwards. Diffusion fluxes, specifically those involving grain boundary diffusion, are necessary for stage (iv) mass transport between particles in contact and give rise to interparticle bonding and sintering. Therefore, an increase

in the rate of sintering and interparticle bonding at a given temperature when applying a cyclic pressure could be expected, compared to constant pressure SPS.

4.3 Microstructural evolution during static and cyclic pressure sintering

In the previous section we have suggested a mechanism for the effect of cyclic pressure application on densification and interparticle bonding. Evidence for this proposed mechanism can be seen in the fracture surface features of Figs. 7 and 8 where there is clear evidence for enhanced deformation and enhanced sintering of particles in sample processed by cyclic SPS. The dwell time of 60 minutes will allow more complete densification by mass transport mechanisms. (see ref. [36] for details). Evidence for this is seen at 500 and 600 °C in the fracture surfaces features of Fig. 9 where enhanced interparticle bonding with a 60 min dwell is revealed. On the other hand, for the sample sintered at 400 °C which was found to be brittle, interparticle bonding was insufficient to provide significant ductility. A possible reason is that the grain boundary diffusion and surface diffusion coefficients of α-Ti decrease by one to two orders of magnitude between 400 and 500 °C, as predicted from the diffusion data presented in [36].

It is also important to examine the effect of dwell time on the grain size evolution. In those samples where the dwell temperature was below 500 °C the difference in grain size between 0 min dwell and 60 min dwell was not significant, probably because the Ti remained in the α phase (transition temperature for pure Ti is around 890 °C) with a low diffusion coefficient which implies that the rate of grain growth will be low [36]. However, in the samples sintered at 600 and 700 °C with a 60 min

dwell under cyclic pressure, more grain growth was observed compared to the constant pressure condition at the same temperatures. Although the temperature is still significantly lower than the α-β phase transformation temperature the diffusion coefficient will be higher than at 500 °C and this might suggest that cyclic deformation also introduced lattice defects that enhanced the diffusion coefficient and hence increased the rate of grain growth.

4.4 Sintering parameters and mechanical properties

As shown in Table 3, the Young's modulus of the sintered samples is in the range 96 – 111 GPa, which is slightly lower but in reasonable agreement with data on grade 1 CP-Ti (100 – 103 GPa) according to references [35, 50]. The values of the UTS of samples from the present study are greater than those that are typically reported for grade 1 CP-Ti. The UTS values in the present work range from 422 to 460 MPa and typical literature values are ~ 350 MPa [50]. The values of elongation to failure are also greater than typical literature data for grade 1 CP-Ti. The range in the present work is 27 to 41% for SPS samples with a cyclic pressure and typical literature values are ~30% [35, 50]. (There is one lower value of 25% for the sample with SPS parameters of 600 °C/100 MPa which also had the lowest UTS. This which probably suggests a higher level of porosity than other cyclic SPS samples). However, one needs to be cautious when directly comparing the elongation to failure values across reports in the literature, as these are dependent upon sample geometry (i.e. gauge length) and this is particularly significant for materials with low rates of work hardening, such as the CP-Ti studied here.

The tensile properties can also be compared with data reported by Zadra *et al*. [10] on grade 1 CP-Ti produced by conventional SPS. They reported a range of properties that depended on sintering temperature in the range 700 to 1150 °C and found that the maximum yield stress and ultimate tensile strength occurred after sintering between 750 and 850 °C, with values of ~ 350 and 450 MPa respectively. However, the best ductility was achieved at temperatures above 950 °C, ~ 45%. It is clear from Table 3 that in the present work the low temperature (500 °C) sample with a cyclic pressure of 300 MPa and 60 min dwell achieved very similar results (347 MPa, 458 MPa and 40%).

The effect of using the lowest temperature sintering of 500 °C/300 MPa and 60 min dwell versus conventional SPS sintering at 900 °C in the present experimental equipment is revealed in Fig. 14. The engineering stress-strain curves are shown in Fig. 14 (a) and tensile properties of the samples are listed in Table 3. Clearly, by applying cyclic pressure with a dwell time, sintering at 500 °C/300 MPa allowed us to achieve material with the mechanical properties including UTS and ductility equivalent or superior to that of the conventionally sintered powder. Optical images of the longitudinal sections of the failed specimens after the miniaturized tensile test are shown in Fig. 14 (b). It can be clearly confirmed that both the samples exhibited good tensile ductility and have a significant reduction in area at the failure strain. Fig. 14 (c) shows the inverse pole figure (IPF) maps of these two sintered samples before tensile testing. A significant grain coarsening took place during the 900 °C sintering, on the other hand, the grain size remained fine and equiaxed grain after the cyclic pressure sintering at 500 °C. Thus the low temperature cyclic pressure sintering of CP-Ti powder can prepare the materials

having excellent mechanical properties, equivalent or superior to those of conventional SPS and retain a very fine grain structure.

5. Conclusions

In this study, SPS of CP-Ti was performed under constant and cyclic pressures (cyclic SPS) from 100 to 500 MPa, over a range of temperatures from 400 to 900 °C and with and without a 60 min dwell. The following main conclusions were drawn:

(1) The application of cyclic pressure gives enhanced densification of the CP-Ti powder over the entire range of parameters investigated compared with a constant pressure SPS process. Specifically, cyclic SPS achieves over 99.5 % of the theoretical density even at low temperatures (< 700 °C). The grain size is changed depending on the sintering conditions. That is, under the cyclic SPS conditions of 500 °C/300 MPa/60 min dwell, the grain size is around 10 μm in contrast to approximately 40 μm after conventional SPS at 100 MPa and 900 °C.

(2) Bend testing of samples reveals improved ductility after cyclic SPS compared with equivalent constant pressure processing. A dwell time of 60 min under pressure at the maximum temperature in the sintering cycle leads to a further enhancement of bend test ductility. The miniaturized tensile test results indicate that the cyclic SPS conditions of 500 °C/300 MPa and a dwell time of 60 min at the sintering temperature give the best mechanical properties; a Young's Modulus of 111 GPa, a 0.2 % proof stress of 347 MPa, an ultimate tensile strength of 458 MPa and an elongation to failure of 40 %.

(3) Cold compaction (room temperature) experiments, analyzed by the Cooper-Eaton equation [46], show that cyclic pressure has most probably improved the packing density of powder particles and increased plastic deformation at the points of contact during the low temperature stage of SPS. It is suggested that an increase in the number and size of the points of contact could contribute to enhanced rates of sintering and densification during cyclic SPS.

Overall, cyclic-SPS increases the densification rate of CP-Ti powder, improves the ductility of bend test samples, and gives good mechanical properties. In other words, ultralow temperatures (500-600 °C) sintering of CP-Ti becomes possible by using cyclic pressure application. Whilst the lowest temperature cyclic SPS (500 °C/300 MPa) with an isothermal dwell (60 min) may not be the most economically advantageous in industrial practice, a higher temperature (600 °C but still below the α-β hexagonal to cubic phase transformation) can be selected for faster processing with minimal mechanical property loss. Low temperature cyclic SPS is also effective in obtaining fine equiaxed grains without complex heat treatments because the low temperature process does not involve the α-β phase transformation. It also has a potential to facilitate the preparation of novel types of reinforced Ti-based composites because chemical reactions between the matrix and the reinforcement could potentially be avoided.

Acknowledgments

This work was supported in part by the Next Generation TATARA Project sponsored by the Government of Japan and Shimane Prefecture. It was also supported by the Japan Society for the Promotion of Science, JSPS KAKENHI Grant Number JP21K04712.

Declaration of Competing Interest

The authors declare that they have no known competing financial interests or personal relationships that could have appeared to influence the work reported in this paper.

Appendix A: Experimental method of the compression test

Cold compression tests were performed using the same powder and SPS apparatus as the sintering experiments. The cold compression test was performed at room temperature with cyclic pressures in the range 0 ↔ 20 ~ 500 MPa under a chamber pressure of <10 Pa. The number of applied pressure cycles, *N,* was 1, 3, 10, 100 and 1000 times under a frequency of approximately 0.25 Hz. Die and punches were made of a WC-FeAl, as in the sintering experiments. The density of the resulting Ti compacts was estimated by measuring the thickness of the green compacts. In addition, tap and apparent powder densities were measured to evaluate the compaction mechanism of the powder.

Appendix B: Analysis of the densification process by applying cyclic pressure based on the Cooper-Eaton equation.

In the Cooper-Eaton equation [46], the fractional volume compaction, F_V, is expressed as a function of the applied pressure P (MPa) as follows:

$$F_V = A_1 \exp\left(-\frac{B_1}{P}\right) + A_2 \exp\left(-\frac{B_2}{P}\right) \quad \text{(A1)}$$

The dimensionless constants A_1 and A_2 are the fractional of contribution from rearrangement of particles and plastic deformation, respectively. The constants with a dimension of pressure B_1 and B_2 ($B_1 < B_2$) correspond to the pressures at which the rearrangement and plastic deformation occur, respectively.

In equation (A1), the first and the second terms in the right-hand side are interpreted as the behaviors due to the mechanisms of rearrangement (filling the large voids) and plastic deformation (filling the small voids) in the case of powder compaction process, respectively.

In the present study, F_V was estimated from the density from the following equation (A2):

$$F_V = \frac{D_\infty}{D_P} \cdot \frac{D_P - D_0}{D_\infty - D_0} \tag{A2}$$

D_0 is the compact density at zero pressure, that is the apparent density (2560 kg/m^3), $D_\infty$is the compact density at infinite pressure, that is the theoretical density (4506 kg/m^3) and $D_P$is the compact density at an applied pressure P. The fitting was performed by using a nonlinear least squares method. The Cooper–Eaton model was a good fit to the experimental data with an r-squared value exceeding 0.99.

References

[1] M. Omori, Mater. Sci. Eng. A 287 (2000) 183-188. https://doi.org/10.1016/S0921-5093(00)00773-5

[2] Z. A. Munir, D. V. Quach, M. Ohyanagi, J. Am. Ceram. Soc. 94 (2011) 1-19. https://doi.org/10.1111/j.1551-2916.2010.04210.x

[3] O. Guillon, J. Gonzalez-Julian, B. Dargatz, T. Kessel, G. Schierning, J. Räthel, Adv. Eng. Mater. 16 (2014) 830-849. https://doi.org/10.1002/adem.201300409

[4] R. Orrù, R. Licheri, A. M. Locci, A. Cincotti, G. Cao, Mater. Sci. Eng. R 63 (2009) 127-287. https://doi.org/10.1016/j.mser.2008.09.003

[5] J. Trapp, B. Kieback, Powder Metall. 62 (2019) 297-306. https://doi.org/10.1080/00325899.2019.1653532

[6] J. Garay, Current-activated, Annu. Rev. Mater. Res. 40 (2010) 445-468. https://doi.org/10.1146/annurev-matsci-070909-104433

[7] Z. Hu, Z. Zhang, X. Cheng, F. Wang, Y. Zhang S. Li, Mater. Des. 191 (2020) 108662. https://doi.org/10.1016/j.matdes.2020.108662

[8] N. S. Weston, B. Thomas, M. Jackson, Mater. Sci. tech., 35 (2019) 1306-1328. https://doi.org/10.1080/02670836.2019.1620538

[9] M. Tokita, Ceramics 4 (2021) 160-198. https://doi.org/10.3390/ceramics4020014

[10] M. Zadra, F. Casari, L. Girardini, A. Molinari, Powder Metall. 51 (2008) 59-65. https://doi.org/10.1179/174329008X277000

[11] M. Eriksson, Z. Shen, M. Nygren, Powder Metall. 48 (2005) 231-236. https://doi.org/10.1179/174329005X71939

[12] G. T. Motsi, S. Guillemet-Fritsch, G. Chevallier, M. B. Shongwe, P. A. Olubambi, C. Estournes, Powder Technol. 345 (2019) 415-424. https://doi.org/10.1016/j.powtec.2019.01.005

[13] O. Ertorer, T. D. Topping, Y. Li, W. Moss, E. J. Lavernia, Metall. Mater. Trans. A 42 (2011) 964-973. https://doi.org/10.1007/s11661-010-0499-5

[14] . R. Chaudhari, R. Bauri, Metallogr. Microstruct. Anal. 3 (2014) 30–35. https://doi.org/10.1007/s13632-013-0112-6

[15] J. Shon, J. Park, K. Cho, J. Hong, N. Park, M. Oh, Trans. Nonferrous Met. Soc. China 24(2014) s59−s67. https://doi.org/10.1016/S1003-6326(14)63289-1

[16] M. S. Asl, A. S. Namini, A. Motallebzadeh, M. Azadbeh, Mater. Chem. Phys. 203 (2018) 266-273. https://doi.org/10.1016/j.matchemphys.2017.09.069

[17] J. Kozlík, P. Harcuba, J. Stráský, H. Becker, J. Šmilauerová, M. Janeček, Mater. Charact. 151 (2019) 1-5. https://doi.org/10.1016/j.matchar.2019.02.035

[18] J. Kozlík, H. Becker, J. Stráský, P. Harcuba, M. Janeček, Mater. Sci. Eng. A 772 (2020) 138783. https://doi.org/10.1016/j.msea.2019.138783

[19] A. Miklaszewski, D. Garbiec, K. Niespodziana, Adv. Powder Technol. 29 (2018) 50-57. https://doi.org/10.1016/j.apt.2017.10.010

[20] N. S. Weston F. Derguti, A. Tudball, M. Jackson, J. Mater. Sci. 50 (2015) 4860-4878. https://doi.org/10.1007/s10853-015-9029-6

[21] J. Shon, I. Song, K. Cho, Y. Park, J. Hong, N. Park, M. Oh, Int. J. Precis. Eng. Manuf. 15 (2014) 643-647. https://doi.org/10.1007/s12541-014-0382-1

[22] C. Yang, S. Ni, Y. Liu, M. Song, Mater. Sci. Eng. A 625 (2015) 264-270. https://doi.org/10.1016/j.msea.2014.12.015

[23] D. A. Porter, K. E. Easterling, M. Y. Sherif, Phase Transformations in Metals and Alloys, Fourth ed., CRC Press, Boca Raton (2021). https://doi.org/10.1201/9781003011804

[24] B. Xu, R Fu, Y. Li, J. Ma, B. Yan, Mater. Lett. 282 (2021) 128852. https://doi.org/10.1016/j.matlet.2020.128852

[25] J. Bustillos, C. Zhang, A.a Loganathan, B. Boesl, A. Agarwal, Adv. Eng. Mater. 22 (2020) 2000076. https://doi.org/10.1002/adem.202000076

[26] H. Kitagawa, K. Nagao, N. Mimura, S. Morito, K. Kikuchi, J. Electron. Mater. 43 (2014)1574-1579. https://doi.org/10.1007/s11664-013-2796-4

[27] A. Suzuki, H. Kitagawa, K. Hirayama, A. H. Pham, S. Morito, T. Etoh, K. Kikuchi, J. Electron. Mater. 49 (2020) 2832-2837. https://doi.org/10.1007/s11664-019-07867-3

[28] A. Suzuki, H. Kitagawa, A. H. Pham, S. Morito, K. Kikuchi, Materialia 14 (2020) 100914. https://doi.org/10.1016/j.mtla.2020.100914

[29] K. Gao, Y. Hu, Z. Zhang, C. Ren, W. Zhao, D. Sun, Y. Gao, L. An, Q. Kong, Adv. Eng. Mater. 26 (2024) 2301326. https://doi.org/10.1002/adem.202301326

[30] K. Wang, K. Zhao, J. Liu, D. Liu, T. Li,W. Li, Z. Sun,L. An, Ceram. Int. 47 (2021) 20731. https://doi.org/10.1016/j.ceramint.2021.04.063

[31] T. Zhu, Z. Xie, Y. Han, S. Li, Y. Li, D. An, X. Luo, J. Am. Ceram. Soc. 101 (2017) 1397. https://doi.org/10.1111/jace.15341

[32] A. Suzuki, K. Kikuchi, K. Nakano, H. Kitagawa, J. Jpn. Soc. Powder Powder Metall. 67 (2020) 525-528 (in Japanese). https://doi.org/10.2497/jjspm.67.525

[33] S. Diouf, A. Molinari, Powder Technol. 221 (2012) 220-227. https://doi.org/10.1016/j.powtec.2012.01.005

[34] Y. F. Yang, M. Qian, Spark plasma sintering and hot pressing of titanium and titanium alloys, Titanium Powder Metallurgy: Science, Technology and Applications, Butterworth- Heinemann (2015) 219-235. https://doi.org/10.1016/C2013-0-13619-7

[35] MatWeb Material Property Data. http://www.matweb.com, accessed: April 2024.

[36] R. M. German, Int. J. Refract. Hard Met. 89 (2020) 105214. https://doi.org/10.1016/j.ijrmhm.2020.105214

[37] Z. A. Munir, U. Anselmi-Tamburini, M. Ohyanagi, J. Mater. Sci. 41 (2006) 763-777. https://doi.org/10.1007/s10853-006-6555-2

[38] C. Romaric, L. Gallet Sophie, N. Foad, C. Frédéric, B. Guillaume, F. Gilbert, Jean-Marc, B. Frédéric, J. Alloys Compd. 692 (2017) 478-484. https://doi.org/10.1016/j.jallcom.2016.08.191

[39] Z.-H. Zhang, Z.-F. Liu, J.-F. Lu, X.-B. Shen, F.-C. Wang, Y.-D. Wang, Scripta Mater. 81 (2014) 56-59. https://doi.org/10.1016/j.scriptamat.2014.03.011

[40] D. M. Hulbert, A. Anders, J. Andersson, E.J. Lavernia, A.K. Mukherjee, Scripta Mater. 60 (2009) 835-838. https://doi.org/10.1016/j.scriptamat.2008.12.059

[41] T.M. Vidyuk, D. V. Dudina, M.A. Korchagin, A.I. Gavrilov, T. S. Skripkina, A. V. Ukhina, A.G. Anisimov, B.B. Bokhonov, Vacuum 181 (2020)109566. https://doi.org/10.1016/j.vacuum.2020.109566

[42] R. Liu, W. Wang, H. Chen, Z. Lu, W. Zhao, T. Zhang, Adv. Powder Tech. 30 (2019) 2649-2658. https://doi.org/10.1016/j.apt.2019.08.012

[43] T. Nagae, M. Yokota, M. Nose, S. Tomida, T. Kamiya, S. Saji, Mater. Trans. 43 (2002) 1390-1397. https://doi.org/10.2320/matertrans.43.1390

[44] P. Shewmon, Diffusion in Solids (2nd edition), The Minerals, Metals and Materials Society, Warrendale, PA 1988, 202. https://doi.org/10.1007/978-3-319-48206-4

[45] V. Mamedov, Powder Metall. 45 (2002) 322-358. https://doi.org/10.1179/003258902225007041

[46] A. R. Cooper, L. E. Eaton, J. Am. Ceram. Soc. 45 (1962) 97-101. https://doi.org/10.1111/j.1151-2916.1962.tb11092.x

[47] L. Luo, Y. Sun, Y. Tang, Metals 13 (2023) 360. https://doi.org/10.3390/met13020360

[48] T. Itoh, Y. Wanibe, J. Jpn Soc. Powder Metall. 46 (1999) 16-21. https://doi.org/10.2497/jjspm.46.16

[49] P. Peralta, C. Laird, Cyclic Plasticity and Dislocation Structures, Reference Module in Materials Science and Materials Engineering, Elsevier (2016). https://doi.org/10.1016/B978-0-12-803581-8.02917-9

[50] A. Szkliniarz, W. Szkliniarz, Materials 16 (2023) 711. https://doi.org/10.3390/ma16020711

Figures

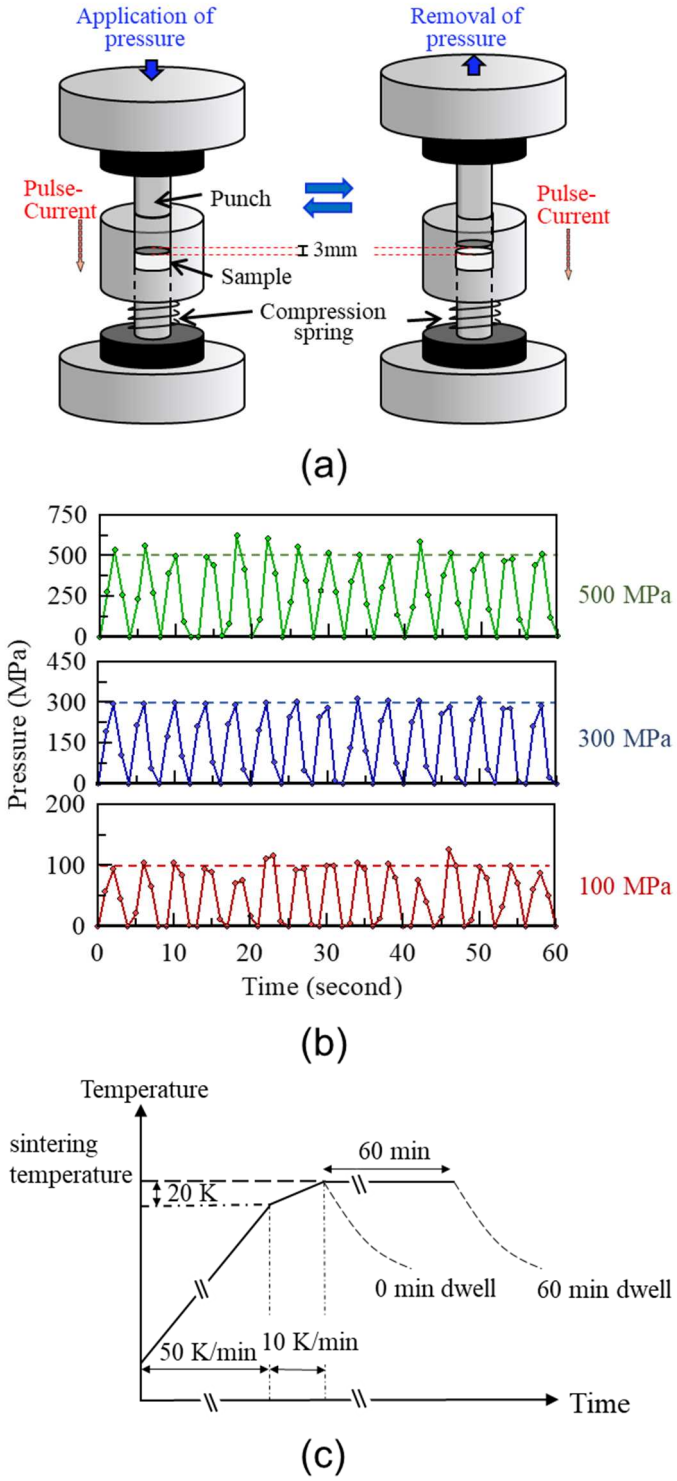

Figure 1 (a) Schematic illustration of the SPS process with an application of cyclic pressure. (b) Typical pressure pattern used for the cyclic SPS process. (c) Schematic temperature programs during the SPS process.

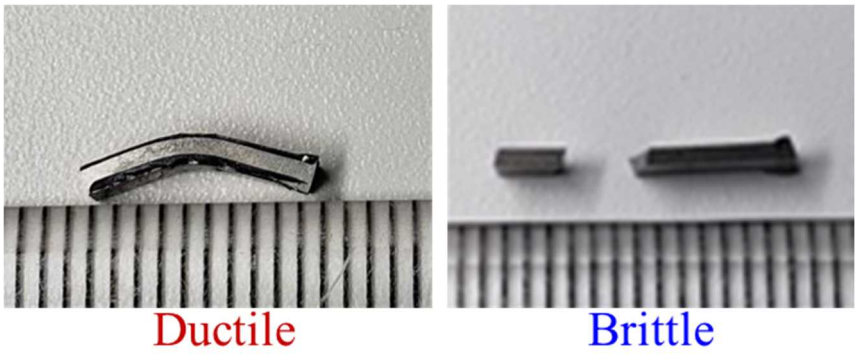

Figure 2 Photographs of representative SPS-processed samples following bending; one is ductile and the other is brittle. Scales are in millimetres.

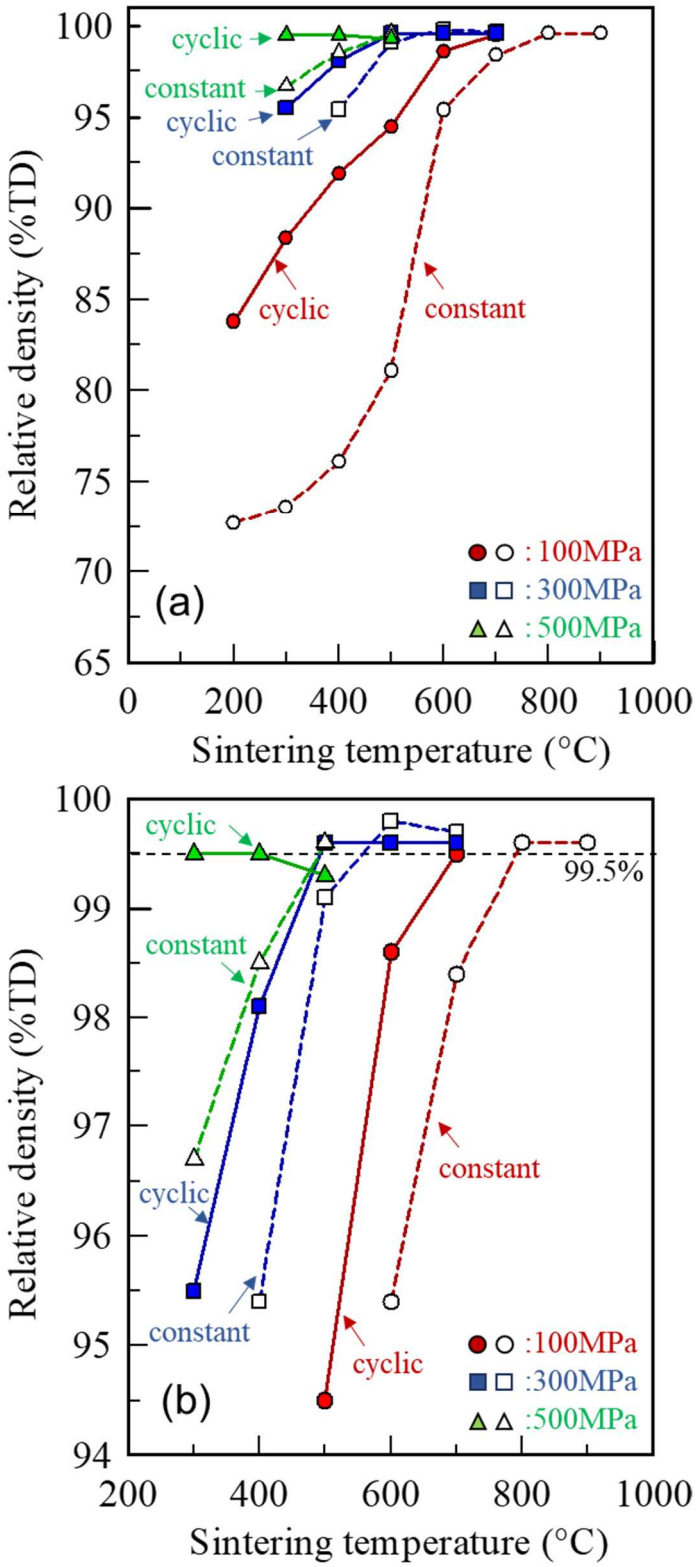

Figure 3 Relative density (% of theoretical density) after SPS of CP-Ti at different temperatures. SPS was performed without an isothermal dwell. (a) Entire measured range, and (b) enlarged section of higher relative density part (>94 % theoretical density).

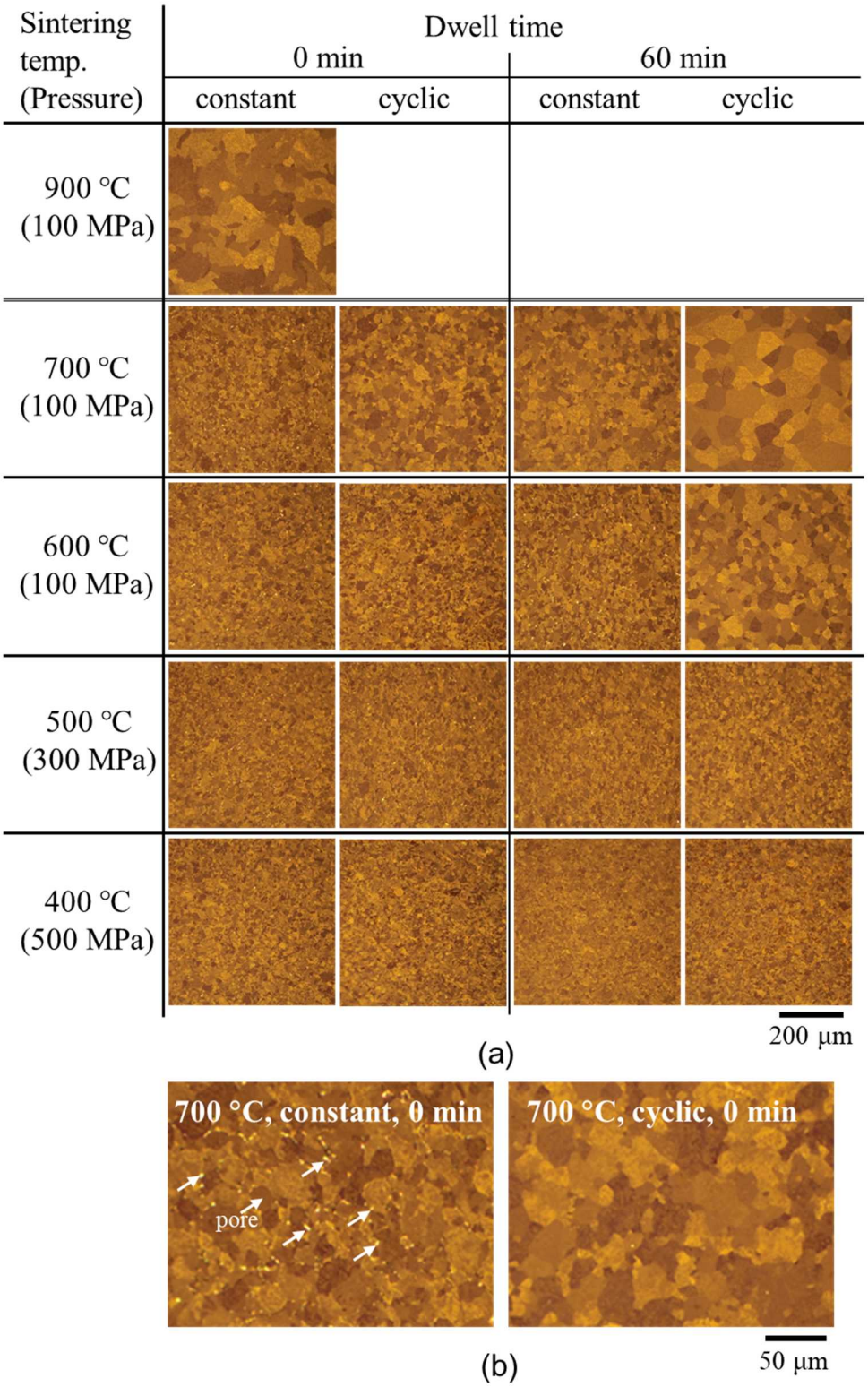

Figure 4 (a) Optical micrographs showing the microstructure of samples sintered at various temperatures under constant and cyclic pressure. Applied pressures were 100 MPa for sintering temperatures ≥ 600 °C, 300 MPa for sintering at 500 °C and 500 MPa for sintering at 400 °C. Dwell time is 0 min and 60 min. (b) The magnified optical micrographs for samples sintered at 700 °C for 0 min under constant and cyclic pressure.

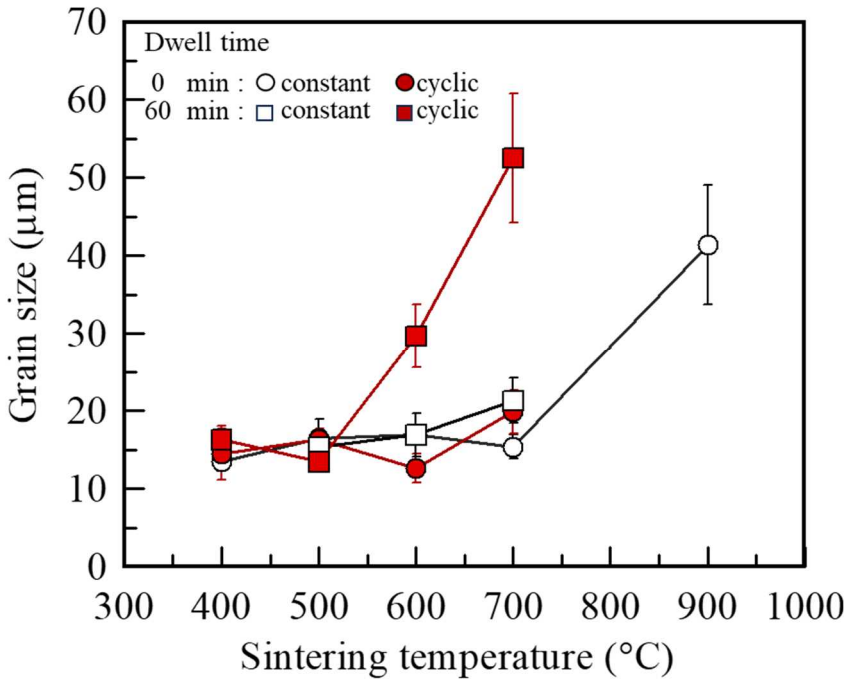

Figure 5 Grain size of samples sintered at 400 - 900 °C under constant and cyclic pressures with 0 or 60 min dwell times.

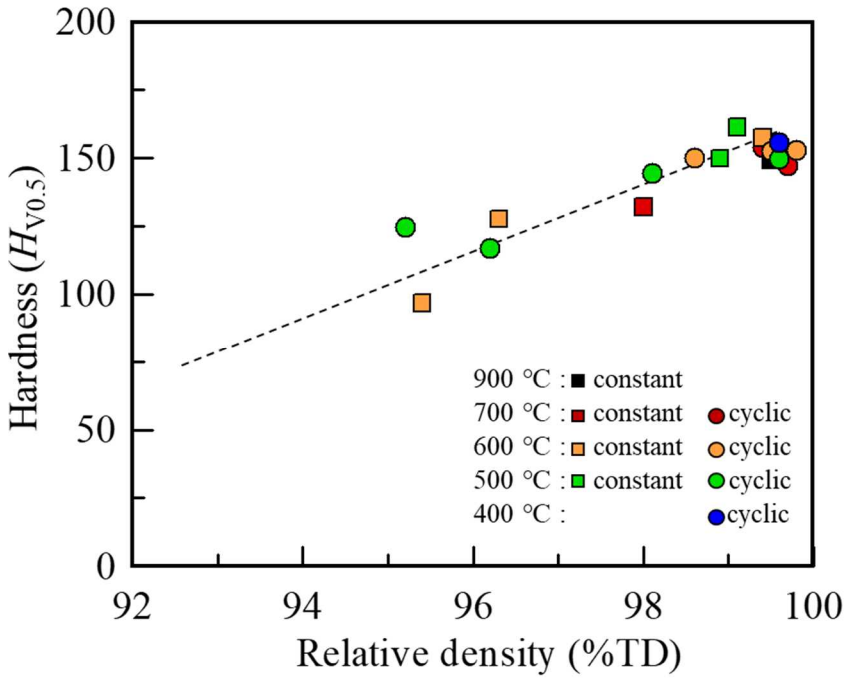

Figure 6 Relationship between Vickers microhardness and relative density for all sintered samples. The dashed line is a trendline.

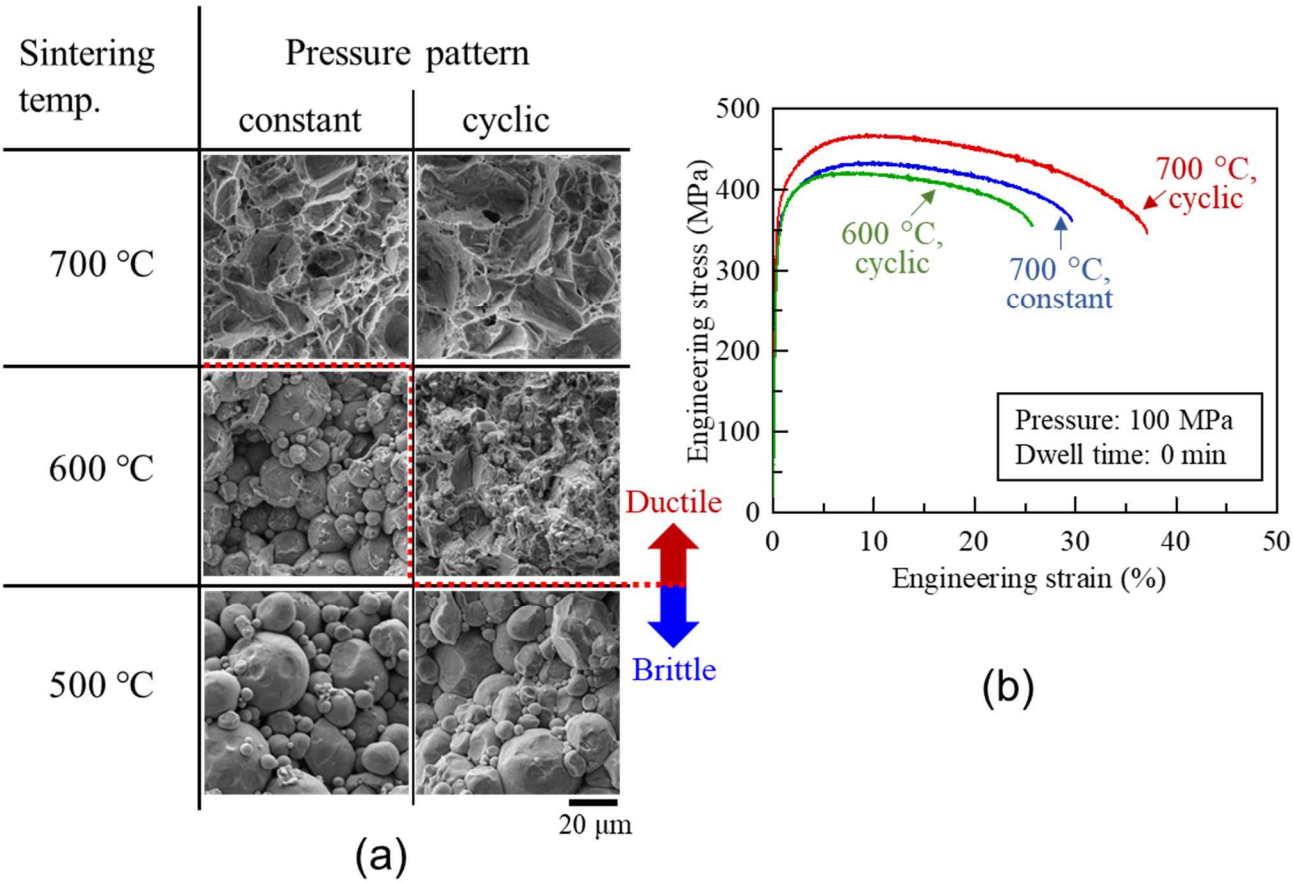

Figure 7 The effect of applying a cyclic versus a constant pressure (100 MPa) at three different sintering temperatures on the mechanical behavior (without an isothermal dwell).

(a) SEM images of fracture surfaces following bending of samples prepared by SPS at 500 - 700 °C under 100 MPa.

(b) Engineering stress-strain plots for different processing conditions at 100 MPa.

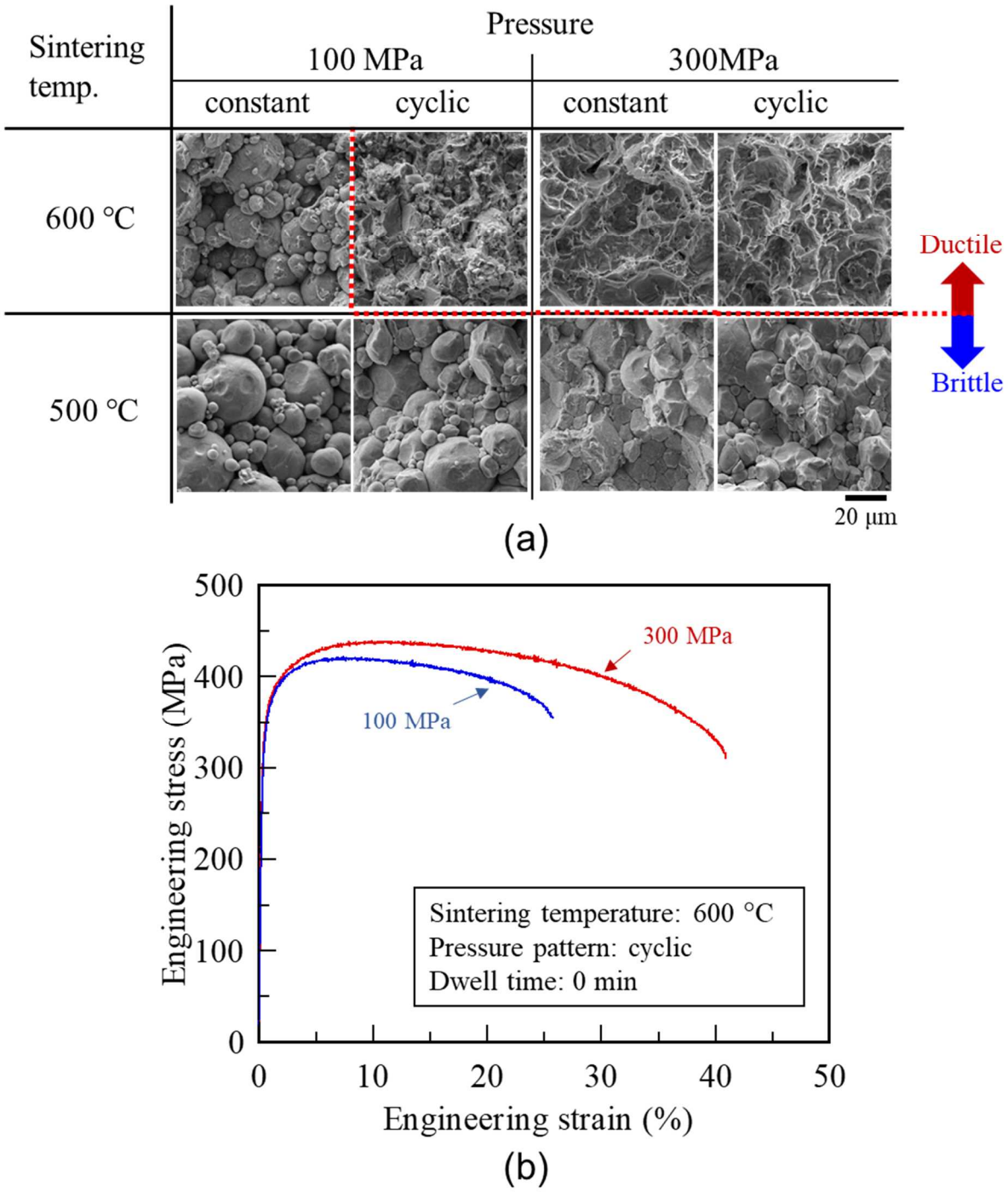

Figure 8 The effects of the applied pressure and temperature on the mechanical behavior (without an isothermal dwell).

(a) SEM images of fracture surfaces following bending of samples prepared by SPS at 500 and 600 °C under 100 and 300 MPa.

(b) Engineering stress-strain plots for cyclic pressures of 100 and 300 MPa (600 °C).

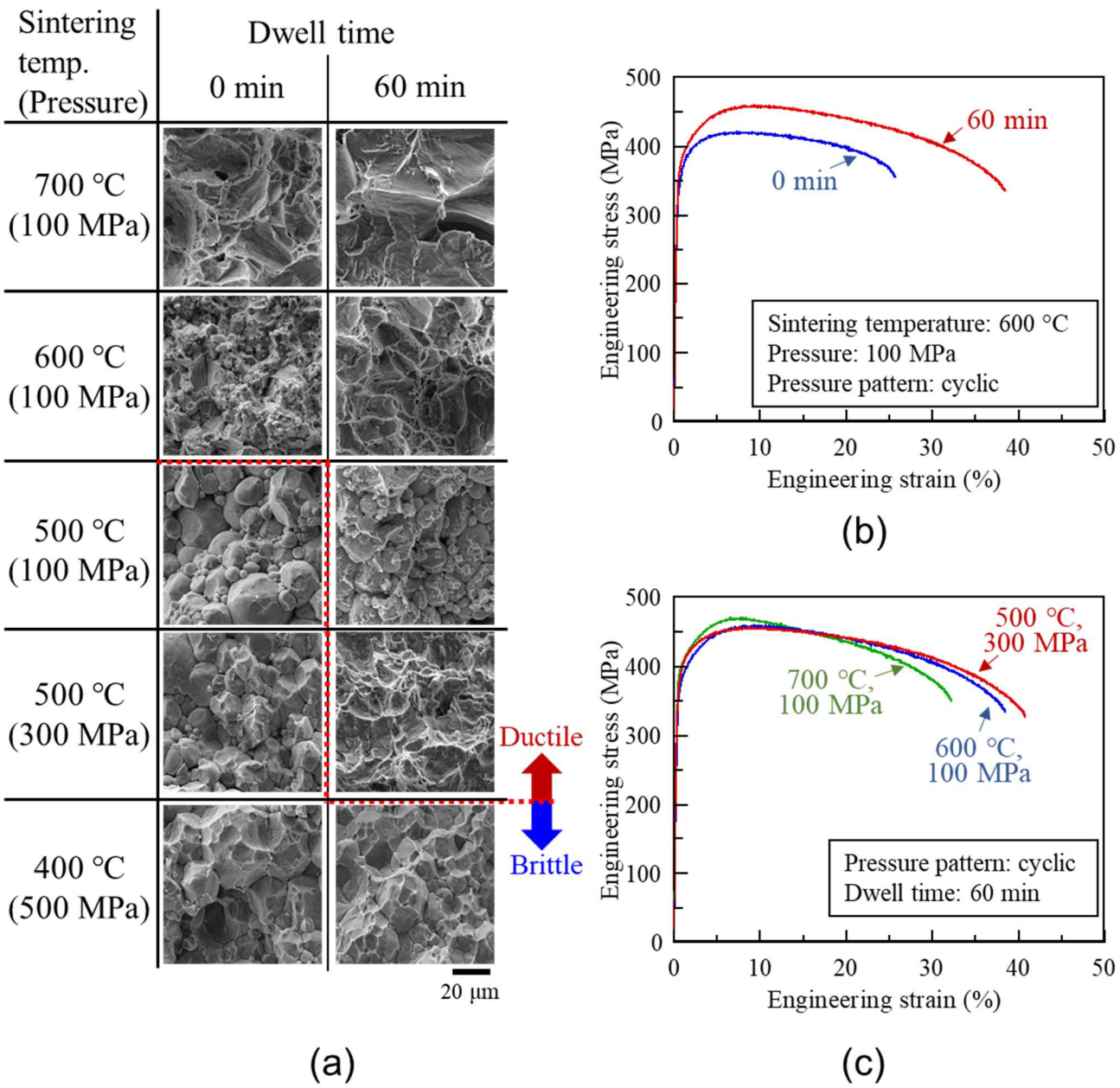

Figure 9 The effects of dwell time and sintering temperature on the mechanical behavior when a cyclic pressure is applied. (a) SEM images of fracture surfaces following bending of samples prepared by SPS at 400 - 700 °C under 100 - 500 MPa with and without a dwell time. (b) Engineering stress-strain plots for the effect of dwell time (600 °C, 100 MPa, cyclic pressure). (c) Engineering stress-strain plots comparing the effects of cyclic pressure and temperature with a 60 min dwell.

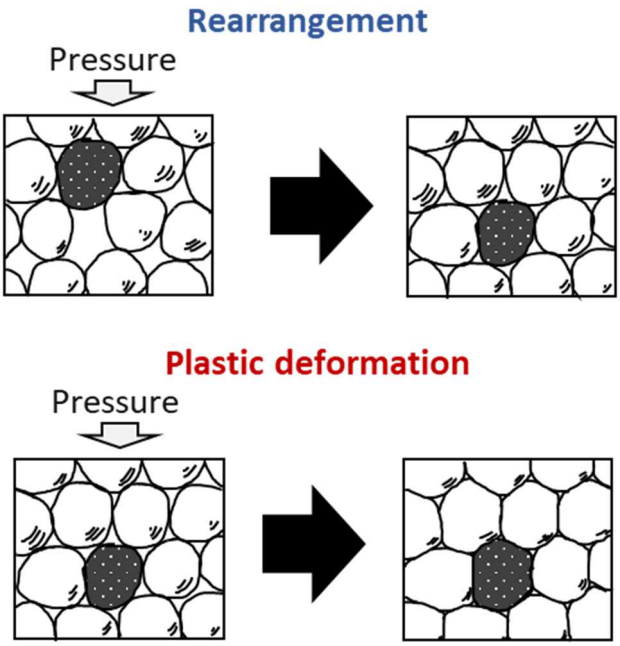

Figure 10 Schematic illustration of the mechanism of powder rearrangement and plastic deformation during powder consolidation under pressure.

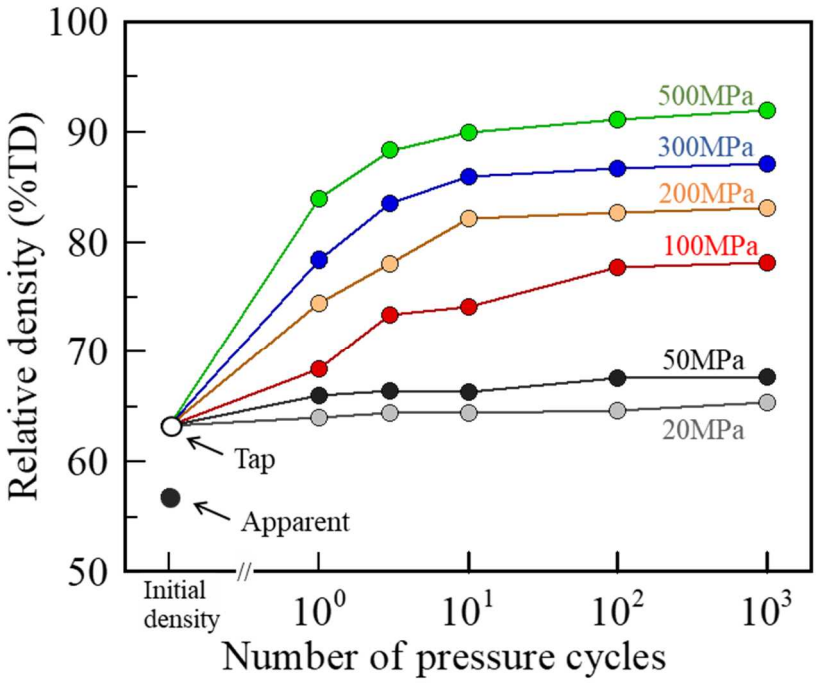

Figure 11 Plot showing the relative density of CP-Ti powder compacts versus the number of pressure cycles for different pressure values from 20 to 500 MPa at room temperature.

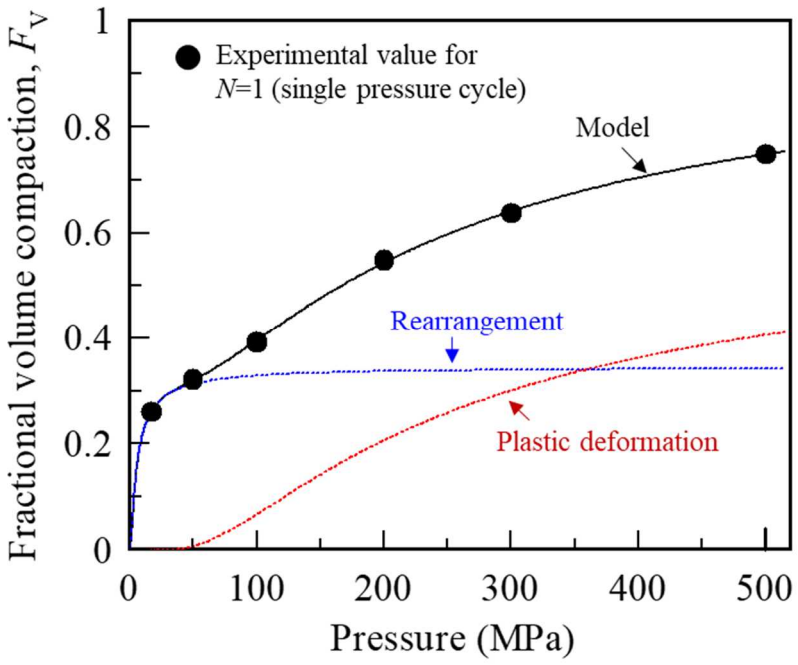

Fig. 12 Plot of fractional volume compaction F_V for single pressure cycle (N=1) versus applied pressure for room temperature compaction of Ti powder showing the powder deformation and powder rearrangement components calculated from the experimental data using the Cooper-Eaton equation (A1).

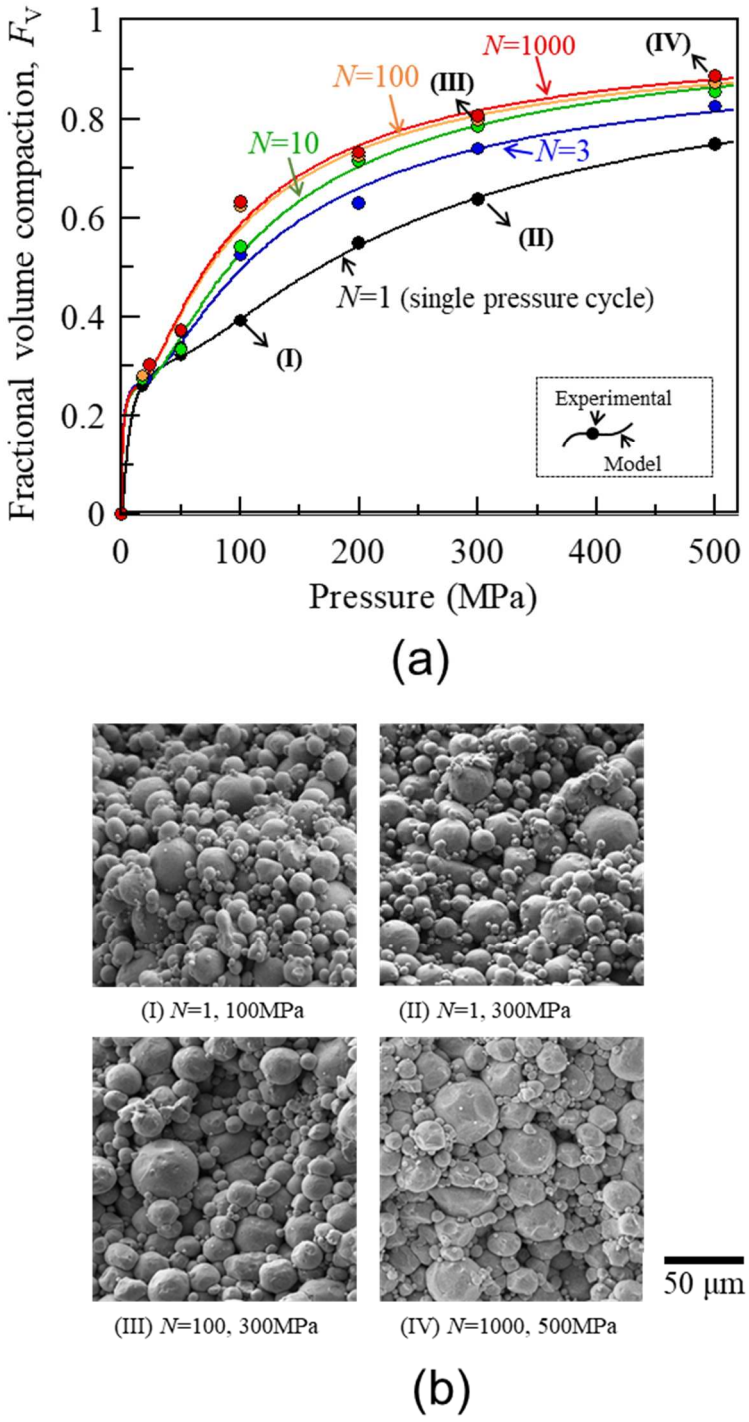

Fig. 13 (a) Plot of fractional volume compaction F_V versus applied pressure for room temperature compaction of Ti powder classified by the number of applied pressures (N=1, 3, 10, 100, 1000). Closed circles are the experimental value, and dotted and solid lines represent the fitted curves based on the Cooper-Eaton equation (A1). (b) the SEM images of the compressed powder at the four points (I, II, III, IV) indicated by arrow in (a).

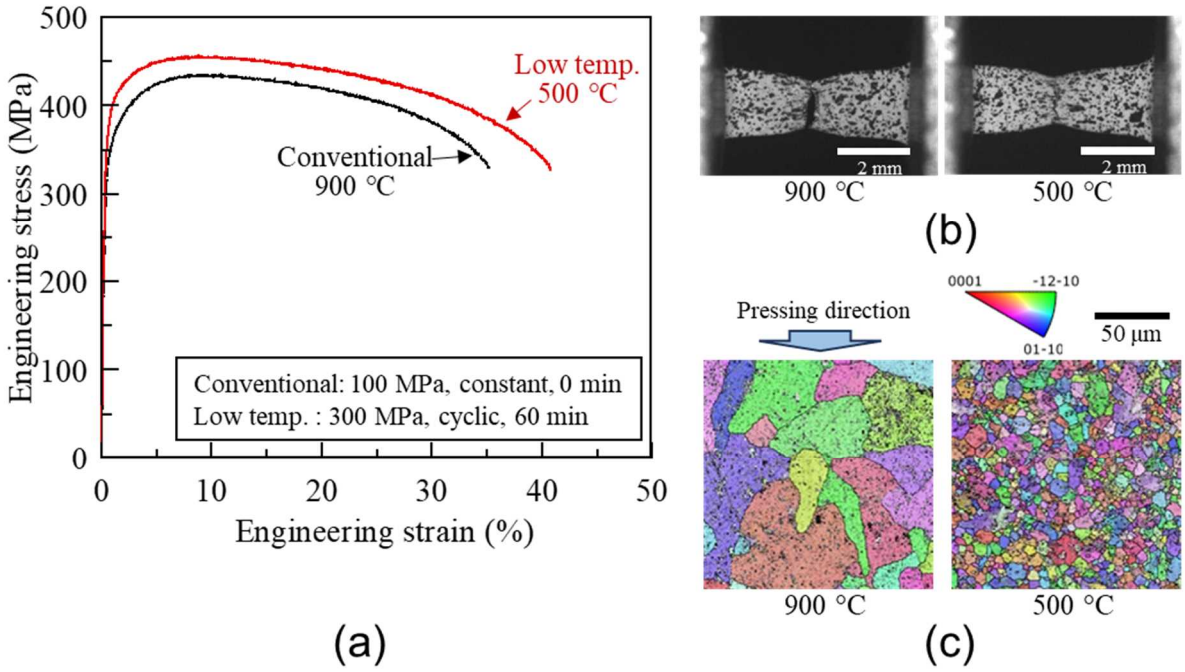

Fig. 14 Comparison between conventional 900 °C/100 MPa SPS of Ti with a processing cycle comprising 500 °C/300 MPa and 60 min dwell. (a) Engineering stress-strain plots; (b) Optical microscope images of longitudinal sections of representative tensile test pieces after failure. (c) EBSD derived inverse pole figure (IPF) maps revealing the different grain sizes in the samples before tensile testing. The color indicates crystallographic orientation of pressing direction.